PCCP

PAPER

View Article Online
View Journal | View Issue

Cite this: *Phys. Chem. Chem. Phys.*, 2015, **17**, 14138

Time-resolved IR spectroscopy of a trinuclear palladium complex in solution†

M. Zimmer,[a] F. Rupp,[b] P. Singer,[b] F. Walz,[c] F. Breher,*[c] W. Klopper,*[d] R. Diller*[b] and M. Gerhards*[a]

Received 14th February 2015,
Accepted 24th April 2015

DOI: 10.1039/c5cp00959f

www.rsc.org/pccp

This paper presents a combined spectroscopic and theoretical analysis of a trinuclear $[Pd_3\{Si(mt^{Me})_3\}_2]$ complex (mt^{Me} = methimazole) which has been demonstrated to be a potential catalyst for coupling reactions. It is a highly symmetric model system (D_3 in the electronic ground state) for the investigation of electronic states and the structure of polynuclear transition metal complexes. Different time-resolved IR spectroscopic methods covering the femtosecond up to the microsecond range as well as density functional computations are performed to unravel the structure and character of this complex in the electronically excited state. These are the first time-resolved IR studies on a trinuclear Pd complex. Based on the interplay between the computational results and those from the IR studies a ^3A state is identified as the lowest lying triplet state which has C_2 symmetry.

1 Introduction

Polynuclear transition metal complexes are known to have chemically interesting properties and applications, *e.g.* in catalysis[1–4] or light harvesting processes,[5,6] which can be explored in photochemical and photophysical investigations.[7–9] The afore-mentioned properties can be influenced by cooperative effects between the metal centers,[10–13] *i.e.* the interactions (couplings) between the metal centers and the ligand(s) have to be investigated. These investigations require versatile spectroscopic techniques and detailed theoretical analyses. In recent years structure-sensitive X-ray[14–18] and vibrational spectroscopy[19–28] with sub-ps up to μs time resolution have been applied to explore structure and dynamics of electronically excited transition metal containing complexes.

In this context a very interesting trinuclear palladium complex[29] (**1**, Fig. 1) has been investigated by our research groups with a variety of state-of-the-art photophysical and computational methods.[30] These analyses gave a detailed insight into the photophysical properties and into the electronically excited states. Based on these investigations we could characterize the lowest lying triplet state from which a long-lived (τ_{Ar} = 1.3–1.7 μs, τ_{Air} = 222 ± 3 ns)[30] luminescence occurs. Extensive theoretical work was involved to obtain conclusions on the electronically excited states of **1**. However, no conclusive investigations on the *structures* of the electronic states have been performed up to now, which would yield more precise information on these states and thus a better and more reliable assignment. For the investigations presented here we use structure sensitive time-resolved IR spectroscopy from the femto- to the microsecond

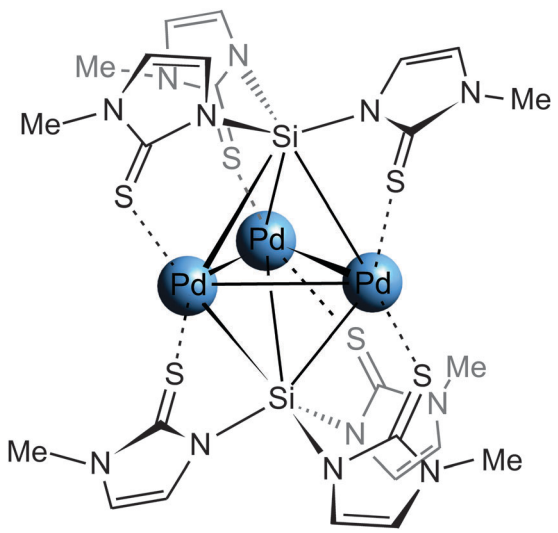

Fig. 1 Structural arrangement of $[Pd_3\{Si(mt^{Me})_3\}_2]$ (**1**).

[a] *Chemistry Department and Research Center Optimas, TU Kaiserslautern, Erwin-Schrödinger-Straße 52, 67663 Kaiserslautern, Germany. E-mail: gerhards@chemie.uni-kl.de; Fax: +49 631 2052750; Tel: +49 631 2052537*
[b] *Physics Department, TU Kaiserslautern, Erwin-Schrödinger-Straße 46, 67663 Kaiserslautern, Germany. E-mail: diller@physik.uni-kl.de; Fax: +49 631 2053902; Tel: +49 631 2052323*
[c] *Institute of Inorganic Chemistry, Karlsruhe Institute of Technology (KIT), Engesserstr. 15, 76131 Karlsruhe, Germany. E-mail: breher@kit.edu; Fax: +49 721 60847021; Tel: +49 721 60844855*
[d] *Institute of Physical Chemistry, Karlsruhe Institute of Technology (KIT), Fritz-Haber-Weg 2, 76131 Karlsruhe, Germany. E-mail: klopper@kit.edu; Fax: +49 721 60847225; Tel: +49 721 60847263*

† Electronic supplementary information (ESI) available. See DOI: 10.1039/c5cp00959f

time range in combination with further theoretical analyses that go beyond our previous work;[30] this is the first application of such a strategy to a trinuclear Pd complex. Our chosen combination of methods is especially suited to analyse the structure of the complex in its ground and excited states.

To cover the nano- and microsecond range, time-resolved step-scan FTIR spectroscopy (TR-FTIR) is applied. Publications of TR-FTIR measurements on transition metal complexes exist since the early 1990s.[22–25] Most of those investigations are about electronically excited states, especially with respect to metal-to-ligand charge transfer (MLCT) transitions in complexes including one or two metal centers. In these early investigations so called "reporter" ligands (carbonyl and cyanide) have been introduced which bear the advantage of a huge oscillator strength for the ν(CO) and ν(CN) stretching vibration(s) and a high sensitivity for structural changes.[22] Investigated systems without a "reporter" ligand are for example Ru(bpy) complexes (bpy = 2,2′-bipyridine) including the well analyzed $[Ru(bpy)_3]^{2+}$.[26,27] Regarding the number of metal atoms very few examples for tri- and tetra-metallic investigations with TR-FTIR can be found in the literature, some of them focus on the energy transfer in rhenium complexes, *e.g.* $[(bpy)(CO)_3Re(trans\text{-}dppene)Re(phen)(CO)_2(trans\text{-}dppene)Re(bpy)(CO)_3]^{3+}$ (phen = phenanthroline, dppene = 1,2-bis(diphenylphosphino)ethene) and $Re_4(CO)_{12}(4,4'\text{-}bpy)_4Cl_4$.[24,28]

Having none of the above mentioned "reporter" groups in our system (**1**) our investigations are even more demanding. The transient (step-scan) FTIR spectroscopy still benefits from the advantages of the FTIR technique among them the possibility to record a complete spectral region simultaneously (multiplex advantage). Thus it is possible to capture the whole mid-IR region (and in principle also NIR and FIR). In our case the mid-IR region, especially from 1600 to 1100 cm^{-1}, is of interest.

After a detector rise time of about 30 ns our step-scan set up enables us to perform measurements with a resolution of about 10 ns (see Section 2). Beyond this, ultrafast transient IR spectroscopy is applied to the trinuclear palladium complex to investigate the primary photoinduced vibrational dynamics in the femto and picosecond time domain, thereby covering the entire excited state lifetime from its very beginning. Femtosecond transient IR spectroscopy has been applied successfully to the investigation of divers photoinduced phenomena in metal complexes such as CO release,[31–33] excited state dynamics in $Cr(acac)_3$[34] and a Ru(II) catalyst[35] as well as high-spin state formation in Fe(II) spin-crossover systems.[21] Thereby ultrafast vibrational dynamics can be related to electronic dynamics as intersystem crossing and internal conversion.[36,37]

2 Experimental methods

The Pd_3 complex (**1**) was prepared following the synthesis described in ref. 29. DMSO-d_6 (<0.02% water, 99.8% D) was purchased from VWR Chemicals and purged with argon prior to usage. All experiments described in Sections 2.1 and 2.2 were performed at room temperature.

2.1 Time-resolved step-scan FTIR spectroscopy

For the time-resolved FTIR experiments a Bruker VERTEX 80v spectrometer equipped with a step-scan interferometer module was used (for a detailed description of the experimental set-up, *cf.* Fig. S1 of the ESI†). The spectrometer, using a liquid-nitrogen cooled mercury–cadmium–telluride (MCT) detector connected to a fast preamplifier, was coupled with a Q-switched Nd:YAG laser (Lumonics HY750, frequency tripled to 355 nm) that generates excitation pulses with a half-width of about 10 ns and a repetition rate of 10 Hz. The timing of the laser pulse and the step-scan triggering was performed by a Stanford Research Systems DG535 delay generator. The UV pump beam was adjusted to have an overlap with the spectrometer's IR probe beam inside the flow cell. To avoid backscattering of the UV pulse into the detector or interferometer compartment, AR-coated germanium filters were placed inside the sample compartment.

A mM solution of **1** in argon purged DMSO-d_6 was pumped by a peristaltic pump (Masterflex Easy-Load II, variable flow rate) through an optical cell that is part of a closed-cycle continuous flow tubing system including a sample reservoir. The cell was composed of housing, CaF_2 windows, separated by two Mylar® spacers with a variable thickness (0.006 to 0.5 mm). In our case 0.26 mm spacers and a flow rate of about 40 mL min^{-1} are chosen. The sample cell as well as the sample reservoir were purged by argon to assure an excited state lifetime of τ_{Ar} = 1.3–1.7 μs, since it is quenched by oxygen to τ_{Air} = 222 ns.[30] The 355 nm excitation laser beam was attenuated to 0.6–0.8 mJ per shot at a diameter of about 9 mm. The temporal resolution was set to 20 ns for these measurements. Five adjacent 20 ns intervals were joined and averaged, so a temporal resolution of 100 ns was obtained. The step-scan experiment was triggered 400 ns before the Q-Switch of the laser was triggered which means that the laser beam reached the sample 600 ns after the experiment starts. Hence this time was set as zero point in all spectra. A total number of 465 coadditions at each interferogram point was recorded. The spectral region was limited by undersampling to 0–2633 cm^{-1} with a spectral resolution of 2 cm^{-1} (resulting in 2665 interferogram points). For the prevention of problems by performing a Fourier transformation an IR longpass filter (transmission 4.73–9.00 μm) was used (*i.e.* no IR intensity outside the measured region should be observed).

Both amplified AC and DC signals of the MCT detector were fed to a 14-bit transient recorder board (Spectrum Germany, M3I4142, 400 MS/s), which in turn was connected to an external computer running Bruker OPUS software for spectrometer control and data manipulation/analysis. For data analysis the recorded DC and AC spectra were used to calculate the ΔA (change in absorbance) spectra with:

$$\Delta A = -\log\left(\frac{AC + DC \times \gamma}{DC \times \gamma}\right) \quad (1)$$

with the factor γ that is compensating for different amplifications of AC and DC channel (for further description, see ESI†). The resulting spectra show peaks with positive and negative sign. Negative bands are bleach bands resulting from the

depletion of ground state vibration. Positive bands belong to vibrations of the excited species.

2.2 Ultrafast transient IR absorption

For femtosecond mid-IR experiments, the complex was dissolved at concentration equivalent to an OD = 2 at 330 nm in dimethylsulfoxide (DMSO) for probe around 1166 cm^{-1} and in deuterated DMSO (DMSO-d_6) for probe around 1453, 1295, 1378 cm^{-1} (see Section 4). The solution was placed between two UV-grade CaF_2 windows (Crystal GmbH) of 2.54 cm in diameter with 250 μm path length. Before and after each femtosecond transient experiment steady state UV/Vis spectra (JASCO, V-670) were recorded to ensure sample integrity.

The femtosecond pump–probe experiments were based on a Ti:sapphire regenerative amplifier system to generate ultrashort pump and probe pulses (CPA-2001, Clark MXR: rep. rate 1 kHz, pulse energy 1 mJ, central wavelength 775 nm, pulse duration 150 fs (FWHM)).

A home-build two stage non-collinear optical parametric amplifier was used to generate femtosecond pump pulses at 330 nm with energy of 250–300 nJ at the sample position. Another portion of the fundamental beam was fed in a two stage optical parametric amplifier with consecutive difference frequency generation, yielding the spectrally tunable probe pulse between 6–12 μm with a spectral width of 50–60 cm^{-1} as described before.[38] Pump and probe pulses were superimposed in the sample with focal width of about 200 and 100 μm, respectively. The sample was rotated to exchange the excited volume between two consecutive laser shots. The transmitted mid-IR probe light was spectrally dispersed and detected by a polychromator with a 32-element MCT (mercury–cadmium–telluride) detector array (Infrared-Systems-Development) with ≈ 2 cm^{-1} spectral width per element. In all experiments the pump beam was chopped at half the repetition rate (500 Hz), allowing the calculation of pump-induced difference absorbance spectra $\Delta OD(\lambda,t)$ on a shot-to-shot basis as a function of probe wavelength and pump–probe delay. Time zero of the experiment was determined *via* a transient absorption experiment on a thin silicon wafer. The pump/probe cross correlation time was typically ≈ 350 fs (FWHM, Gauss).

The transient data was analyzed by a global fit routine, describing the time dependent absorbance change $\Delta OD(\lambda,t)$ as a sum of exponential decay functions

$$\Delta OD(\lambda,t) = A_0(\lambda) + \sum_{i=1}^{n} A_i(\lambda) \cdot e^{-\frac{t}{\tau_i}} \qquad (2)$$

with amplitudes $A_i(\lambda)$ as decay associated spectra (DAS), τ_i as the corresponding time constants and $A_0(\lambda)$ as the difference spectrum after "infinite" delay time.

3 Theory

Quantum-chemical calculations were performed with the TURBOMOLE program package[39] at the level of density-functional theory (DFT) using the hybrid functional B3LYP. The calculations were performed in exactly the same basis as used in ref. 30, that is, dhf-TZVP-2c for Pd, S, and Si, and def2-SV(P) for H, C, and N. This basis is referred to as "TZVP" for short. In ref. 30, the geometries of the $^3A_1$ and $^3A_2$ excited states as well as the $^1A_1$ ground state were optimized in the framework of self-consistent Kohn–Sham calculations (ΔSCF) at the B3LYP/TZVP level in D_3 symmetry. Subsequently, in the course of the present work, we computed the harmonic vibrational frequencies at these geometries using a parallelized version[40] of the module AOFORCE,[41] which allows for the analytical calculation of force constants. For the $^1A_1$ ground state, we have found that all computed harmonic vibrational frequencies are real, meaning that the D_3 equilibrium structure is a true minimum on the potential energy hypersurface. For each of the two triplet excited states, however, we obtained one (two-fold degenerate) imaginary frequency of *e* symmetry ($26i$ cm^{-1} for the $^3A_1$ state and $122i$ cm^{-1} for $^3A_2$). Therefore, these states were re-optimized in C_2 symmetry, now yielding true minima with real harmonic vibrational frequencies. In C_2 symmetry, the $^3A_1$ (D_3) state becomes a ^3A state, whose adiabatic ΔSCF energy is found 1.79 eV above the well depth of the ground state (this value was 1.81 eV for its D_3-symmetric counterpart) while the $^3A_2$ (D_3) state becomes a ^3B state, whose adiabatic energy is found 2.01 eV above the ground state (this value was 2.32 eV in D_3 symmetry). Hence, the energy lowering due to the geometry relaxation in C_2 symmetry amounts to 0.02 and 0.31 eV for the ^3A and ^3B states, respectively. In the ^3A state, the three Pd atoms form an isosceles triangle with two equal sides of 270.2 pm and one longer side of 275.4 pm while in the ^3B state, they form an isosceles triangle with two equal sides of 285.9 pm and one shorter side of 281.3 pm (in D_3 symmetry, the Pd–Pd distances were 271.5 pm and 288.2 pm, respectively, in the $^3A_1$ and $^3A_2$ states).

For gaining insight into the observed energy lowering due to geometry relaxation, we computed a correlation diagram (*cf.* ESI,† Fig. S2) of the frontier orbitals as a function of a distortion coordinate x, which is defined as follows: $x = 0$ corresponds to an unbiased D_3-symmetric geometry that is obtained by averaging the $^3A_1$ and $^3A_2$ geometries optimized in ref. 30; $x = -1$ corresponds to the C_2-symmetric geometry of the ^3B state and $x = +1$ corresponds to the C_2-symmetric geometry of the ^3A state. Separate linear interpolations of the structures are performed between the $x = -1$ and $x = 0$ geometries on the one hand and between the $x = 0$ and $x = +1$ geometries on the other. The LUMO is stabilized for both positive ($x > 0$) and negative ($x < 0$) distortions. This can be understood as pseudo-Jahn–Teller effect[42] due to interactions with a close-lying two-fold degenerate e level (LUMO+1, 72e). At the same time, the HOMO is destabilized towards $x = +1$ while the HOMO−1 is destabilized towards $x = -1$. The latter even becomes the HOMO in the ^3B geometry. The interplay between destabilization of the relevant ground-state occupied orbitals and stabilization of the LUMO appears to be responsible for the energy lowering upon distortion. Consistent with the correlation diagram, Fig. S3 (ESI†) shows the energies of the excited states of interest as a function of the distortion coordinate, as obtained from TDDFT computations at the B3LYP/TZVP level using the lowest triplet state as reference.

The Cartesian coordinates of the ground state and the two triplet states are given in the ESI† (Tables S1–S3).

4 Spectroscopic results and discussion

Static IR spectra

In the spectral region from 1150 to 1550 cm^{-1} four IR absorption bands belonging to **1**, at 1172, 1301, 1383, 1457 cm^{-1} are identified (see Fig. S4, ESI† and lower trace of Fig. 2 in the region down to 1250 cm^{-1}); furthermore a broad, not well structured absorption region from 1390–1450 cm^{-1} is observed. In comparison to the DFT calculations the four defined peaks can be assigned to $\delta(C–H)_{aliphatic}$ 1457 cm^{-1} (1454 cm^{-1}), $\nu(C–N)$ 1301 cm^{-1} (1300 cm^{-1}) and skeletal vibrations 1383 and 1172 cm^{-1} (1379 and 1159 cm^{-1}), calculated values in parentheses (scaling factor 0.98, see below).

Nano- and microsecond time regime

After laser excitation five bleach bands appear at 1174, 1303, 1385, 1402 and 1458 cm^{-1} (Fig. 2 and 3) in the step-scan FTIR spectrum, which can definitely be assigned to the electronic ground state vibrations. (Remark: the values observed in depletion differ by a few wavenumbers from the values obtained in the static FTIR spectrum due to a significant spectral overlap of the ground- and electronically excited state vibrational bands. This is illustrated in Fig. S5, ESI†). In addition, four new bands appear that are 9–14 cm^{-1} red shifted at 1162, 1289, 1373 and 1449 cm^{-1}. These bands originate from the electronically excited species. Furthermore the relative depletion intensities of the ΔA peaks match that of the steady state spectrum (see Fig. 2 and Fig. S6, ESI†).

In the first 100 ns interval after excitation the bands at 1303/1289, 1385/1373 and 1458/1449 cm^{-1} are already observable (see inset of Fig. 2). To obtain a better S/N ratio and since no dynamics in this temporal range are visible spectra are also averaged to 500 or 1000 ns steps. The signal disappears completely after about 3.5 μs, confirming the TCSPC lifetime measurements[30] and giving a hint that the argon purged sample chamber and argon purged housing of the sample reservoir prevent the sample from oxygen. (For a better illustration of the decay within microseconds, the transient IR spectra up to 3.5 μs are shown in steps of 500 ns in the ESI,† *cf.* Fig. S7).

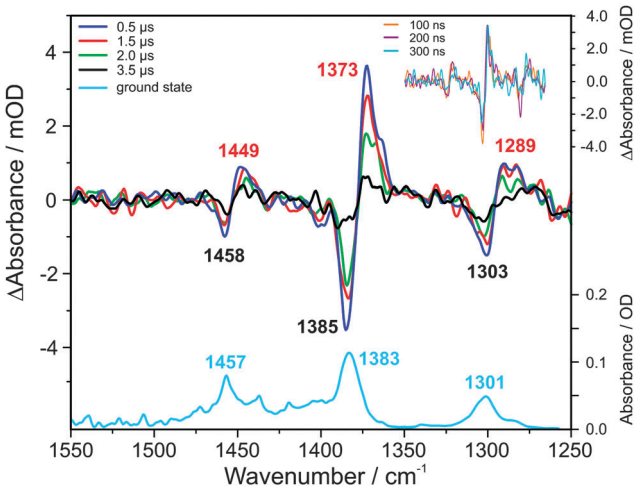

Fig. 2 Bottom: steady state FTIR, solvent DMSO-d_6 subtracted; top: TR-FTIR spectra, 0.5, 1.5, 2.0 and 3.5 μs after excitation at 355 nm; inset: TR-FTIR spectra, 0.1, 0.2 and 0.3 μs after excitation at 355 nm.

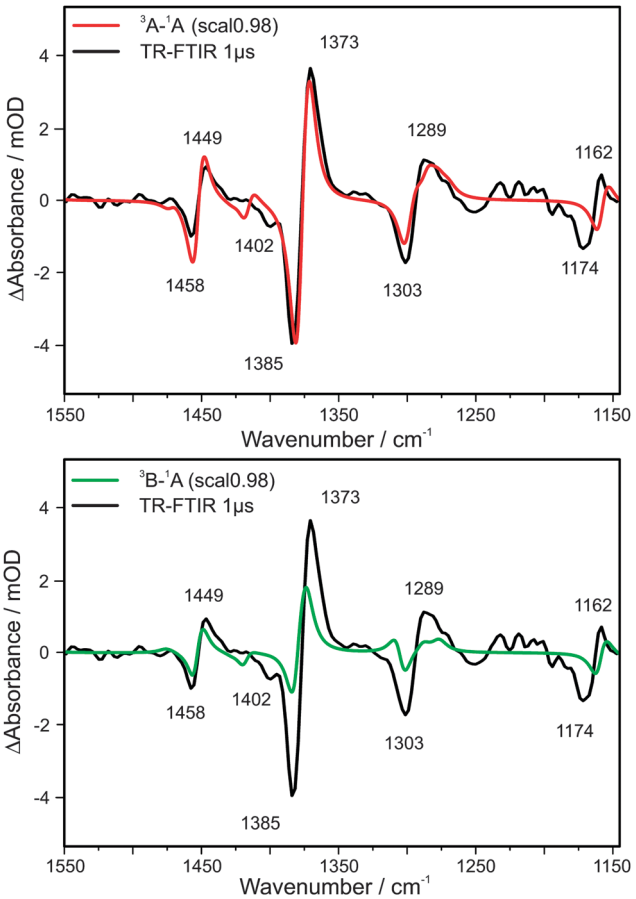

Fig. 3 TR-FTIR spectrum 1.0 μs after excitation; top: in comparison with calculated excitation into a ^{3}A state; bottom: in comparison with calculated excitation into a ^{3}B state.

In order to compare calculated harmonic frequencies with experimental values the computed vibrational frequencies have to be scaled. A typical empirical factor for the chosen theoretical ansatz (*cf.* Section 3) is 0.98 (*cf. e.g.* ref. 43). The reliability of this factor can be tested by fitting the calculated IR spectrum of the electronic ground state (^{1}A) as well as the spectra of the electronically excited states (^{3}A and ^{3}B) to the experimental values. Indeed the best agreement is achieved for a factor of 0.98. (In case of the ^{3}A state the scaling factors vary between 0.979 and 0.983 whereas for the ^{3}B state the variation is larger, between 0.970 and 0.983, indicating a better description of the experimental frequencies for the ^{3}A state.)

In the DFT calculations a red shift of the ^{3}A state vibrations compared to the ground state ^{1}A (modes) in the order of about 10 cm^{-1} is observable, for example 16 cm^{-1} for the 1285/1301 cm^{-1} peaks or 7 cm^{-1} for the 1373/1380 cm^{-1} peaks (Fig. S8). In contrast, the vibrational modes of the ^{3}B state are closer to the values of the ^{1}A state. It should be mentioned that the investigated spectral region shows small but significant differences for the calculated ^{3}A and ^{3}B spectra. Other parts of the spectrum are either less significant or cannot be observed with our experimental set-ups (*cf.* Fig. S9 of the ESI†).

In order to quantify the comparison between calculated and experimentally observed frequencies the calculated spectrum of the electronic ground state (^{1}A) has to be subtracted from the calculated spectra obtained for the ^{3}A and ^{3}B states. In order to simulate the vibrational spectra, Lorentzian functions are used. By fixing the band positions (scaling factor 0.98), different full widths at half maximum (FWHM) are chosen. By testing a constant width or variable widths (between 10 and 20 cm^{-1}) within one fit it turns out that 14 cm^{-1} is the best average value. The goodness of the fit can be described by the R^2/χ^2 parameter which is about a factor of three to four better for the ^{3}A state compared to ^{3}B (by using a scaling factor of 0.98 and a constant band width of 14 cm^{-1} or a variable band width between 10 and 20 cm^{-1} optimized for each transition). Fig. 3 shows the comparison of experiment and theory: Fig. 3 (top) ground state (^{1}A) subtracted from ^{3}A and Fig. 3 (bottom) ^{1}A subtracted from ^{3}B. It can be seen that the calculated band positions (relative to the experimental values) are better predicted for the ^{3}A state, especially in the case of the transitions at 1289, 1373 and 1449 cm^{-1}. In case of the ^{3}B state also an additional band around 1310 cm^{-1} would be expected which is not observed in the experimental spectrum. Furthermore, the calculated difference spectra reveal also that only the ^{3}A state gives an appropriate description of the experimentally observed band intensity ratios, especially for the transitions at 1373/1385 cm^{-1}. In case of this most prominent pair of transitions both increase and depletion in the ΔA spectrum are of similar intensity for the ^{3}A state (in agreement with the experiment) whereas for the ^{3}B state the increase should be by a factor of 3 larger than the depletion. Taking the qualitative and quantitative aspects of calculated frequencies and intensities into account, it can be concluded that the excited state probed on the nano- and microsecond time scale is a ^{3}A state.

Another experiment was performed with a frequency doubled Nd:YLF laser (edgewave INNOSLAB IS8 II – ET, output of about 0.4 mJ per shot at 261.5 nm) that was operated at 100 Hz. According to our previous experimental study[30] it is known that the UV/Vis spectrum shows two strong and broad absorptions: the first electronic transition has its maximum around 333 nm and a second one is around 262 nm. By exciting the second electronic transition with a wavelength of 261.5 nm, the same IR transitions as for the excitation of the first electronic transitions (with 355 nm) are observed in the step-scan FTIR spectrum. These finding clearly show that after electronic excitation the same long-lived electronic state is reached.

Femto- and picosecond time regime

In our earlier work,[30] femtosecond transient absorption in the UV/Vis already showed the ultrafast formation of an electronically excited state within much less than 1 ps with no subsequent spectral changes up to 700 ps. In order to investigate the formation of this long lived state *via* its IR spectrum transient IR spectroscopy is performed. Fig. 4 (top) displays IR difference absorption signals at selected delay times of 0.5 and 340 ps after photoexcitation at 330 nm between 1145 and 1480 cm^{-1}. Fig. 4 (bottom) depicts two kinetic traces at 1366 and 1381 cm^{-1}.

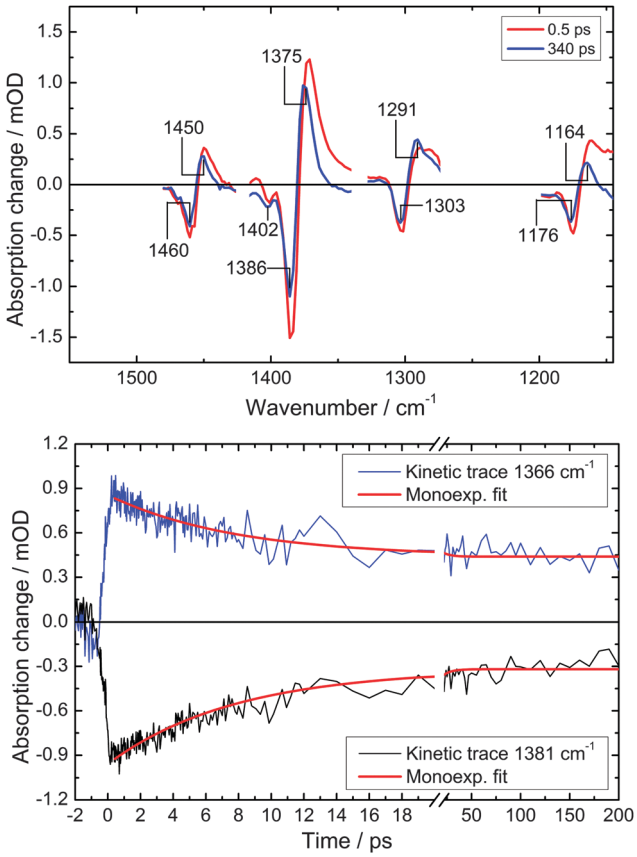

Fig. 4 Top: mid-IR difference absorption spectra at selected delay times (0.5 and 340 ps) after photoexcitation at 330 nm. Wavenumbers indicate the (apparent) peak positions at 340 ps. Bottom: kinetic trace at 1366 cm^{-1} (blue) and 1381 cm^{-1} (black) and global monoexponential fit with τ_1 = 7.8 ± 0.4 ps (red).

They show that after instantaneous absorption rise and bleach, respectively, the signal decreases within a few picoseconds and merges into stationary amplitude.

The stationary difference spectrum at 340 ps exhibits negative peaks at 1176, 1303, 1386, 1402 and 1460 cm^{-1} and positive peaks at 1164, 1291, 1375 and 1450 cm^{-1}. As in the TR-FTIR spectra the bleach peaks (neg.) are assigned to the electronic ground state and the positive vibrational bands are assigned to the long living excited state, the latter showing a rather uniform bathochromic shift of about 10 cm^{-1} with respect to the former. The difference spectrum at early times (0.5 ps) is very similar to that at 340 ps, however, the respective difference bands are of larger amplitude with increased positive absorbance on the low-energy side. This feature is easily explained by vibrational cooling, *i.e.* the dissipation of the excess energy to the solvent: Anharmonic coupling between thermally populated low-energy vibrational modes and high-energy modes (fingerprint region) causes asymmetrically broadened vibrational bands. Thus, the observed apparent blue-shift on the picosecond time scale indicates the cooling process of the vibrationally hot (unrelaxed) molecule in the excited electronic state. It should be noted that the spectral shapes (widths) of the positive bands in the transient spectra are not uniform since they are determined by band-specific parameters

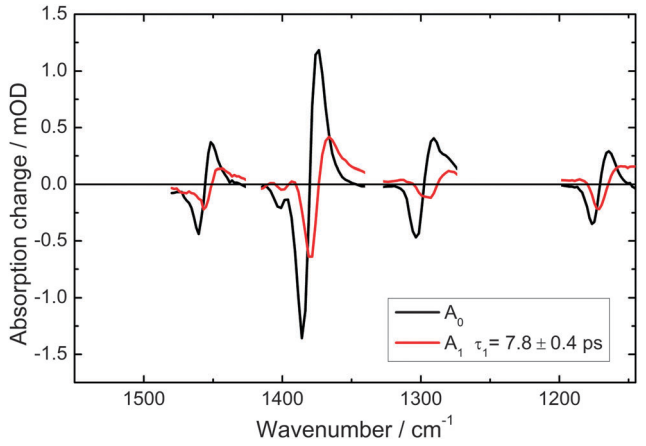

Fig. 5 Decay associated mid-IR spectra (DAS, according to eqn (2)), describing the cooling process ($A_1(\lambda)$) and the "stationary" difference absorption spectrum ($A_0(\lambda)$) (*cf.* text for details).

such as (1) spectral width (dephasing time) of the particular band in the excited electronic state and (2) the anharmonic coupling constants of the particular band to all other vibrational modes in the excited electronic state, especially to the low frequency modes.

Although the relation between vibrational temperature and time-dependency of the observed spectral changes is intrinsically non-exponential, the global fit according to eqn (2) is used in order to derive a characteristic time constant. This yields τ_{VR} = 7.8 ± 0.4 ps with the decay associated spectrum $A_1(\lambda)$ given in Fig. 5. It now describes the observed blue-shift of each product vibrational band (Fig. 4) in terms of monoexponentially decaying positive (low energy lobe) and negative (high energy lobe) absorbance strength as an approximation for the cooling process. $A_0(\lambda)$ is basically identical with the 340 ps difference spectrum, confirming the quality of the fit. Note the excellent match of $A_0(\lambda)$ and the microsecond-FTIR spectra (Fig. 3). No further, sub-ps time constant (as found in the transient UV/Vis data reported earlier (380 fs)[30]) could be derived from the data. This might be due to the highly transitory character of the Franck–Condon state, leading to spectrally extremely broad infrared bands with possibly low absorption cross section. In addition the given (limited) time resolution and S/N-ratio add to this effect. Thus the IR data together with the transient UV/Vis data reported earlier (ref. 30) indicate that ultrafast intersystem-crossing (ISC), internal conversion (IC) and thermalization *via* intramolecular vibrational relaxation (IVR) lead to the vibrationally hot ^{3}A excited state within less than 400 fs. Subsequently the excess energy of about 15 500 cm^{-1} (according to λ_{exc} = 330 nm and λ_{Fluor} = 675 nm[30]) is dissipated into the solvent.

The ultrafast dynamics, *i.e.* ISC within a few hundred femtoseconds followed by vibrational cooling on the picosecond time scale is typical for photoexcited transition-metal complexes[36] and has been frequently reported.[21,35] In addition, it turns out that the femtosecond transient IR spectra, by their strongly structured spectra, allow for a much clearer identification of the cooling/relaxation process as compared to broad and unstructured UV/Vis spectra, where corresponding spectral broadening and shifts are often much weaker or not even detectable as in our earlier work[30] on this complex.

5 Conclusions

This paper reports on the first characterization of electronically excited states in a trinuclear Pd complex investigated by a combination of time-resolved IR spectroscopy and quantum chemical calculations. Step-scan FTIR and femtosecond IR spectroscopy are chosen to cover a time range from femtoseconds to microseconds. The same vibrational spectrum is obtained for the whole time range (from some ps to about 2 μs) indicating that within less than 400 fs a long-lived electronic state is populated. From the TR-FTIR spectra the decay time of this long-lived excited state obtained *via* luminescence spectroscopy is confirmed. Quantum chemical calculations performed for the excited electronic states show that the lowest energy state is of ^{3}A symmetry. Calculated IR spectra for the optimized ^{3}A state match very well with the experimentally observed ones in contrast to the spectra calculated for the energetically higher ^{3}B state. Thus an unambiguous assignment of the experimentally observed long-lived triplet state to a ^{3}A state can be given in addition to the assignment *via* excited state electronic absorption.[30]

Furthermore the femtosecond transient IR data reveal vibrational cooling characterized by a monoexponential time constant of 7.8 ps and no further changes up to 1 ns. Thus the vibrational excess energy dissipates on a picosecond time scale.

The presented extensive spectroscopic and theoretical studies on a highly symmetric trinuclear Pd complex allow an assignment of electronically excited states and its dynamical behaviour. A long-lived electronically excited state is formed by interaction of the three Pd atoms. The geometry of the complex changes from D_3 symmetry in the electronic ground state to C_2 symmetry in the ^{3}A excited state, *i.e.* a pseudo-Jahn–Teller effect is observed. The trinuclear Pd complex has proved to be a rewarding object to study photophysics of a oligonuclear metal complex by the interplay of experiment and theory. The application of a variety of spectroscopic methods (UV/Vis, luminescence, molecular beam)[30] including now the structure sensitive IR techniques in combination with high level DFT and TDDFT calculations provide a detailed analysis on the structural changes by going from the electronic ground to an electronically excited state. These investigations are a starting point for further examples of interacting metal centers which can be of photophysical, magnetic or catalytical relevance.

Acknowledgements

Financial support by the German Science Foundation (DFG) and Collaborative Research Center CRC/Transregio 88, "Cooperative effects in homo- and heterometallic complexes (3MET)" is gratefully acknowledged (Projects B4, C1, C2, C4).

Notes and references

1 H. B. Gray and A. W. Maverick, *Science*, 1981, **214**, 1201.
2 F. Y. Pétillon, P. Schollhammer, J. Talarmin and K. W. Muir, *Coord. Chem. Rev.*, 1998, **178–180**, 203–247.
3 D. C. Powers and T. Ritter, *Acc. Chem. Res.*, 2012, **45**, 840–850.
4 M. H. Pérez-Temprano, J. A. Casares and P. Espinet, *Chem. – Eur. J.*, 2012, **18**, 1864–1884.

5 S. Serroni, S. Campagna, F. Puntoriero, F. Loiseau, V. Ricevuto, R. Passalacqua and M. Galletta, *C. R. Chim.*, 2003, **6**, 883–893.
6 J. A. Faiz, R. M. Williams, M. J. J. Pereira Silva, L. De Cola and Z. Pikramenou, *J. Am. Chem. Soc.*, 2006, **128**, 4520–4521.
7 T. Suzuki, T. Nakagawa, K. Ohkubo, S. Fukuzumi and Y. Matsuo, *Chem. Sci.*, 2014, **5**, 4888–4894.
8 S. Tschierlei, M. Presselt, C. Kuhnt, A. Yartsev, T. Pascher, V. Sundström, M. Karnahl, M. Schwalbe, B. Schäfer, S. Rau, M. Schmitt, B. Dietzek and J. Popp, *Chem. – Eur. J.*, 2009, **15**, 7678–7688.
9 B. Dietzek, W. Kiefer, J. Blumhoff, L. Böttcher, S. Rau, D. Walther, U. Uhlemann, M. Schmitt and J. Popp, *Chem. – Eur. J.*, 2006, **12**, 5105–5115.
10 I. Bratko and M. Gómez, *Dalton Trans.*, 2013, **42**, 10664–10681.
11 J. Park and S. Hong, *Chem. Soc. Rev.*, 2012, **41**, 6931–6943.
12 R. M. Haak, S. J. Wezenberg and A. W. Kleij, *Chem. Commun.*, 2010, **46**, 2713–2723.
13 O. R. Luca and R. H. Crabtree, *Chem. Soc. Rev.*, 2013, **42**, 1440–1459.
14 N. Huse, H. Cho, K. Hong, L. Jamula, F. M. F. de Groot, T. K. Kim, J. K. McCusker and R. W. Schoenlein, *J. Phys. Chem. Lett.*, 2011, **2**, 880–884.
15 S. E. Canton, K. S. Kjær, G. Vankó, T. B. van Driel, S.-I. Adachi, A. Bordage, C. Bressler, P. Chabera, M. Christensen, A. O. Dohn, A. Galler, W. Gawelda, D. Gosztola, K. Haldrup, T. Harlang, Y. Liu, K. B. Møller, Z. Németh, S. Nozawa, M. Pápai, T. Sato, T. Sato, K. Suarez-Alcantara, T. Togashi, K. Tono, J. Uhlig, D. A. Vithanage, K. Wärnmark, M. Yabashi, J. Zhang, V. Sundström and M. M. Nielsen, *Nat. Commun.*, 2015, **6**, DOI: 10.1038/ncomms7359.
16 C. Bressler, C. Milne, V. T. Pham, A. ElNahhas, R. M. van der Veen, W. Gawelda, S. Johnson, P. Beaud, D. Grolimund, M. Kaiser, C. N. Borca, G. Ingold, R. Abela and M. Chergui, *Science*, 2009, **323**, 489–492.
17 G. Vankó, A. Bordage, M. Pápai, K. Haldrup, P. Glatzel, A. M. March, G. Doumy, A. Britz, A. Galler, T. Assefa, D. Cabaret, A. Juhin, T. B. van Driel, K. S. Kjær, A. Dohn, K. B. Møller, H. T. Lemke, E. Gallo, M. Rovezzi, Z. Németh, E. Rozsályi, T. Rozgonyi, J. Uhlig, V. Sundström, M. M. Nielsen, L. Young, S. H. Southworth, C. Bressler and W. Gawelda, *J. Phys. Chem. C*, 2015, **119**, 5888–5902.
18 S. E. Canton, X. Zhang, L. M. Lawson Daku, A. L. Smeigh, J. Zhang, Y. Liu, C.-J. Wallentin, K. Attenkofer, G. Jennings, C. A. Kurtz, D. Gosztola, K. Wärnmark, A. Hauser and V. Sundström, *J. Phys. Chem. C*, 2014, **118**, 4536–4545.
19 A. L. Smeigh, M. Creelman, R. A. Mathies and J. K. McCusker, *J. Am. Chem. Soc.*, 2008, **130**, 14105–14107.
20 P. Tourón Touceda, S. Mosquera Vázquez, M. Lima, A. Lapini, P. Foggi, A. Dei and R. Righini, *Phys. Chem. Chem. Phys.*, 2012, **14**, 1038–1047.
21 M. M. N. Wolf, R. Gross, C. Schumann, J. A. Wolny, V. Schünemann, A. Døssing, H. Paulsen, J. J. McGarvey and R. Diller, *Phys. Chem. Chem. Phys.*, 2008, **10**, 4264–4273.
22 J. R. Schoonover, G. F. Strouse, K. M. Omberg and R. B. Dyer, *Comments Inorg. Chem.*, 1996, **18**, 165.
23 M. W. George and J. J. Turner, *Coord. Chem. Rev.*, 1998, **177**, 201.
24 J. M. Butler, M. W. George, J. R. Schoonover, D. M. Dattelbaum and T. J. Meyer, *Coord. Chem. Rev.*, 2007, **251**, 492–514.
25 B. D. Moore, M. Poliakoff, M. B. Simpson and J. J. Turner, *J. Phys. Chem.*, 1985, **89**, 850.
26 P. Chen, K. M. Omberg, D. A. Kavaliunas, J. A. Treadway, R. A. Palmer and T. J. Meyer, *Inorg. Chem.*, 1997, **36**, 954.
27 K. M. Omberg, J. R. Schoonover, J. A. Treadway, R. M. Leasure, R. B. Dyer and T. J. Meyer, *J. Am. Chem. Soc.*, 1997, **119**, 7013–7018.
28 A. Gabrielsson, F. Hartl, H. Zhang, J. R. L. Smith, M. Towrie, A. Vlček and R. Perutz, *J. Am. Chem. Soc.*, 2006, **128**, 4253.
29 F. Armbruster, J. Meyer, A. Baldes, P. Ona-Burgos, I. Fernández and F. Breher, *Chem. Commun.*, 2011, **47**, 221.
30 Y. Schmitt, K. Chevalier, F. Rupp, M. Becherer, A. Grün, A. M. Rijs, F. Walz, F. Breher, R. Diller, M. Gerhards and W. Klopper, *Phys. Chem. Chem. Phys.*, 2014, **16**, 8332–8338.
31 T. P. Dougherty and E. J. Heilweil, *Chem. Phys. Lett.*, 1994, **227**, 19–25.
32 P. Rudolf, F. Kanal, J. Knorr, C. Nagel, J. Niesel, T. Brixner, U. Schatzschneider and P. Nuernberger, *J. Phys. Chem. Lett.*, 2013, **4**, 596–602.
33 J. B. Asbury, K. Hang, J. S. Yeston, J. G. Cordaro, R. G. Bergman and T. Q. Lian, *J. Am. Chem. Soc.*, 2000, **122**, 12870–12871.
34 E. M. S. Maôas, R. Kananavicius, P. Myllyperkio, M. Pettersson and H. Kunttu, *J. Am. Chem. Soc.*, 2007, **129**, 8934–8935.
35 D. Imanbaew, Y. Nosenko, C. Kerner, K. Chevalier, F. Rupp, C. Riehn, W. R. Thiel and R. Diller, *Chem. Phys.*, 2014, **442**, 53–61.
36 A. Vlček, *Coord. Chem. Rev.*, 2000, **200**, 933–977.
37 P. S. Wagenknecht and P. C. Ford, *Coord. Chem. Rev.*, 2011, **255**, 591–616.
38 F. Peters, J. Herbst, J. Tittor, D. Oesterhelt and R. Diller, *Chem. Phys.*, 2006, **323**, 109–116.
39 *TURBOMOLE V6.6 2014*, a development of University of Karlsruhe and Forschungszentrum Karlsruhe GmbH, 1989–2007, TURBOMOLE GmbH, 2007, available from http://www.turbomole.com.
40 C. van Wüllen, *J. Comput. Chem.*, 2011, **32**, 1195–1201.
41 P. Deglmann, F. Furche and R. Ahlrichs, *Chem. Phys. Lett.*, 2002, **362**, 511–518.
42 I. B. Bersuker, *Chem. Rev.*, 2013, **113**, 1351–1390.
43 M. K. Kesharwani, B. Brauer and J. M. L. Martin, *J. Phys. Chem. A*, 2015, **119**, 1701–1714.